Asymmetrically Rough Sphere Aerodynamics with Application to Sports Balls

Ryley T. Ohlsen
Masters Student
Stanford Aeronautics and Astronautics
Stanford, California, USA

Advised by:
Juan J. Alonso
Stanford Aeronautics and Astronautics
Stanford, California, USA

Special Thanks to:
Rabi Mehta
Kirsten Wind Tunnel Staff and Crew

Abstract

The aerodynamics of asymmetrically rough spheres is analyzed and a model is developed to predict side force as a function of surface roughness and Reynolds number. The model is then applied to sports ball aerodynamics and predicted and measured forces are compared. The test data collected during a low-speed wind tunnel test show that the side force on a baseball due to asymmetric surface roughness behaves quite interestingly near a Reynolds number of about 1.5×10^5 (corresponding to a ball pitched at about 80 miles per hour). The side force flips direction due to boundary layer behavior near the ball's critical Reynolds number, following a similar (but more dramatic) trend that was found by Mehta (2014).

In Part I, a general overview of spherical aerodynamics is discussed with an emphasis on sports balls. Spherical aerodynamics has a rich history of observation that should serve as a predicate for any new theory development. Generally, ball sports involve spheres that move at speeds near their critical Reynolds number. As a consequence, athletes have empirically developed ways to alter the flight of many sports balls to gain competitive advantages.

In Part II, historical data for roughened spheres are used to develop a theoretical model for the expected side force on an asymmetrically rough sphere as a function of Reynolds number. The model's predictions are then compared to wind tunnel data on cricket balls collected by Mehta (2014).

In Part III, wind tunnel results for asymmetrically scuffed and altered baseballs are discussed. Baseballs were tested at the Kirsten Wind Tunnel at the University of Washington to determine their side force as a function of Reynolds number. Comparison to the theoretical model is also discussed.

In Part IV, applications of the data collected are discussed and related to a pitch's dynamics. It is found that a scuffed baseball has the potential to move anywhere from 5 to 15 inches based on wind tunnel data collected. There is uncertainty in how much a pitch would move due to the effect of rotating seams on a baseball.

In Part V, conclusions and lessons learned are discussed. The model developed to predict side force has potential to be improved if further testing were completed. The baseball data show that the frequent replacement of Major League Baseballs is well-warranted due to the large side force that occurs when the ball is scuffed. In addition, substances applied to a baseballs surface such as pine tar have nearly identical aerodynamic behavior as a scuff and can also cause large lateral movement of pitches. This could unquestionably be used by a pitcher to gain an unfair advantage.

I. Sports-Ball Aerodynamic Overview

Aerodynamics can play a large role in any sport that involves balls moving through air. Tactics to gain a competitive advantage often involve controlling the spin of the ball in a specific way (soccer "bending", baseball curveball, knuckle-ball) or altering the surface roughness of the ball (golf ball dimples, cricket polishing/scuffing, seam location). Each sport has a different Reynolds number regime due to its ball size and speed of travel, therefore each sport has developed different solutions to gain competitive advantages.

The most common way to manipulate the aerodynamic force on a ball is to exploit the so-called Magnus effect. The Magnus effect, credited to the German scientist Gustav Magnus of the late 19th century (Magnus 1852), states that a force is produced by spinning a ball about an axis perpendicular to its line of flight. The force direction is the cross-product of the positive axis of rotation and the direction of flight.

Magnus arrived at his conclusion without understanding the flow characteristics that led to the phenomenon. Interestingly, Newton (1672) noted the Magnus force well before Magnus when he described the effect of spin on a tennis ball. Newton noted, "For, a circular as well as a progressive motion…, it parts on that side, where the motions conspire, must press and beat the contiguous air more violently on than that on the other, and there excite a reluctance and reaction of the air proportionally greater." However primitive early interpretations of the root cause behind the Magnus force were, it became clear after the introduction of the boundary layer concept by Prandtl in 1904 that flow separation was the key to describing the root cause of the force. The physics behind this principle are due to the boundary conditions imposed by a rotating ball. Flow separates earlier on the side of the ball that is moving into the flow because boundary layer momentum is being removed by the moving surface. Conversely, on the side moving with the flow, momentum is added to the boundary layer and it remains attached longer. The asymmetric boundary layer separation creates an asymmetric pressure field around the ball, a net force on the ball, and a wake deflection opposite of the net force on the ball. Figure 1 shows a positive Magnus force on a spinning baseball.

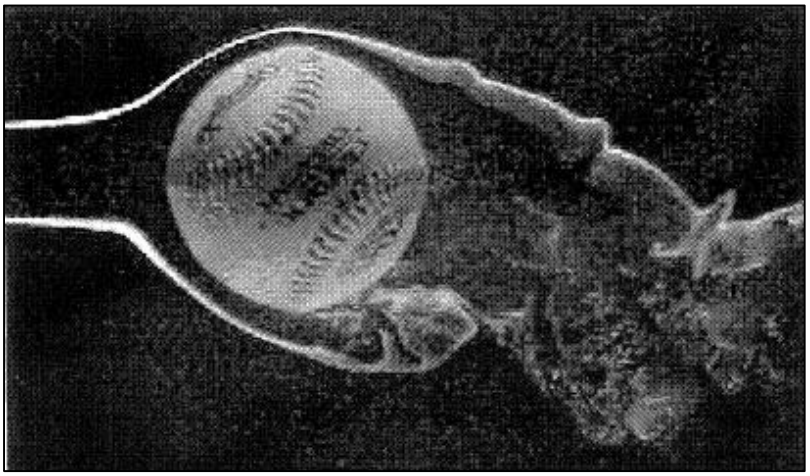

Figure 1 – Wind tunnel flow visualization of a spinning baseball at Re = 3400. Flow is from left-to-right, and ball is spinning in clockwise direction at 0.5 rev/sec. Photograph by Jim Palis. (Mehta Pallis 2001)

Figure 2 depicts a typical smooth-sphere drag coefficient as a function of Reynolds number. It also shows the different flow regimes of a sphere, which represent different Reynolds number ranges where a particular flow characteristic dominates the behavior of flow around the sphere.

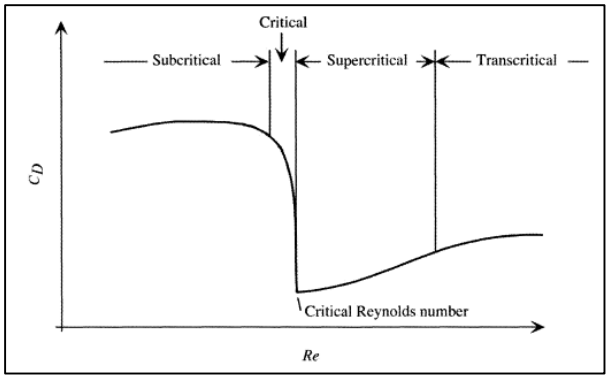

Figure 2 – Flow regimes for a smooth sphere (Mehta & Pallis 2001)

In the subcritical flow regime, the boundary layer on the sphere is laminar up until separation. The laminar flow separates relatively early, and results in a large low-pressure region on the aft side of the sphere. The low-pressure region on the aft side of the sphere is often referred to as the base pressure. The large low base pressure region results in a high drag coefficient of about 0.5 for subcritical spheres. In the supercritical flow regime, the boundary layer along the sphere has transitioned to a turbulent one. As is commonly seen with turbulent boundary layers, the flow remains attached longer and results in a higher base pressure acting on a smaller region of the sphere. The drag coefficient drops to about 1/5 of its subcritical value. The transition to turbulent flow can be brought on either naturally by increasing the Reynolds number, or artificially by using a trip wire, surface roughness, etc. Figure 3 shows the difference between a laminar separation point and a turbulent separation point for a flow around a smooth sphere. In the figure, the transition to turbulent flow was brought on by using a trip-wire instead of increasing the Reynolds number.

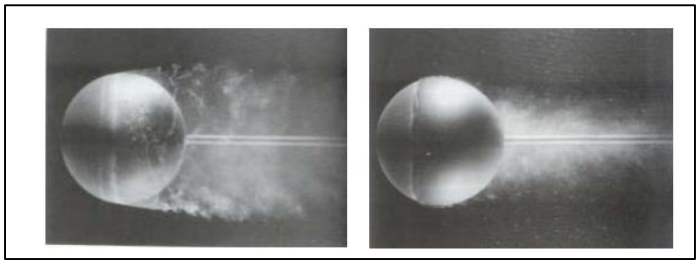

Figure 3 – Laminar separation (left) and turbulent separation (right) for flow around smooth sphere. Turbulent boundary layer is onset by use of trip-wire in photo on right. Credit: John Wiley. (Panton 2005)

It should be noted that the Magnus effect can actually result in a negative Magnus force in flow regimes near a smooth sphere's critical Reynolds number. If the side of the sphere moving into the wind has a relative velocity that results in a supercritical Reynolds number and the side of the sphere moving with the wind has a relative velocity that results in a subcritical Reynolds number, the flow will separate earlier on the side moving with the wind. This deflects the wake in the opposite direction, and gives rise to a negative Magnus force. A depiction of the reverse Magnus effect is shown in Figure 4.

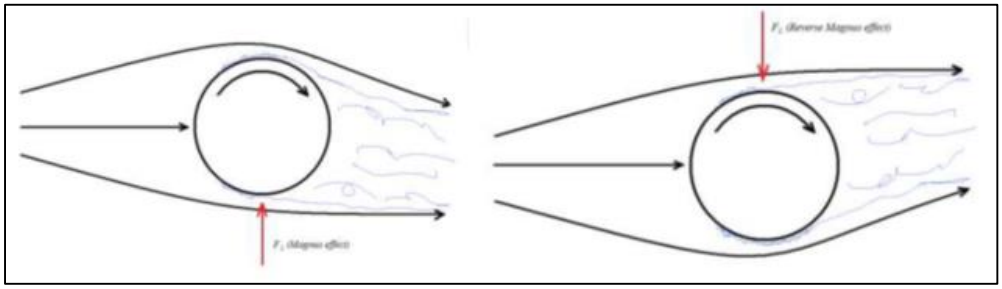

Figure 4 – Depiction of Magnus and reverse Magnus effects. Positive Magnus on left, negative on right. (Kensrud 2010)

This phenomenon has been observed repeatedly on smooth spheres, but is generally elusive for sports balls. Baseballs, in particular, have never been shown to exhibit reverse Magnus forces. This is thought to be due to the stabilizing effect of surface roughness and rotating seams on a baseball. By the time the ball is spinning fast enough to experience a reverse Magnus force, the seams have already changed the flow on both sides to turbulent. This, however, does not mean that a baseball cannot experience situations where only one side is turbulent.

Figure 5 shows how flow past a stationary baseball can result in a net upward force on the ball due to the seam orientation. Flow separation occurs early on the bottom portion of the ball since it is laminar. Flow separation over the top portion of the ball is delayed by turbulence induced by the seams, similar to the trip-wire effect in Figure 3.

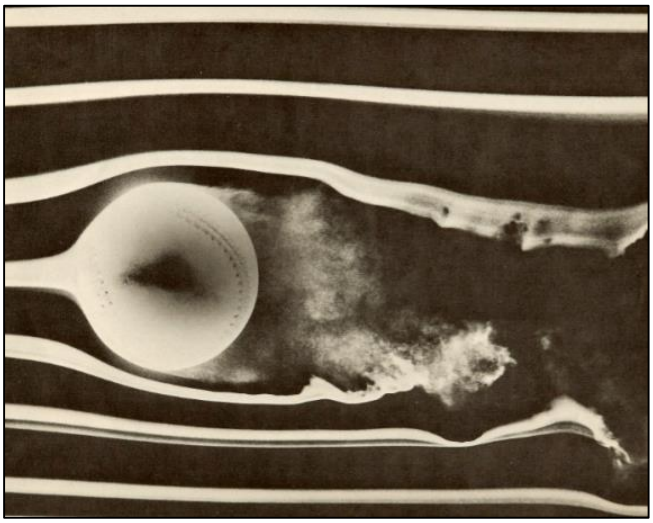

Figure 5 – flow past stationary baseball with both seams oriented on top-half of ball, resulting in wake deflection downward and net upward force on the ball (Brown 1971)

Cricket players also use seams to "swing", or curve, the ball on its way to the batter. A cricket ball contains a single seam down its center. If the ball is pitched in such a way that the seam is tilted relative to its flight path, the flow on the seam-side of the ball will transition to turbulent flow, and the opposite side will remain laminar. This "swing" is depicted in Figure 6.

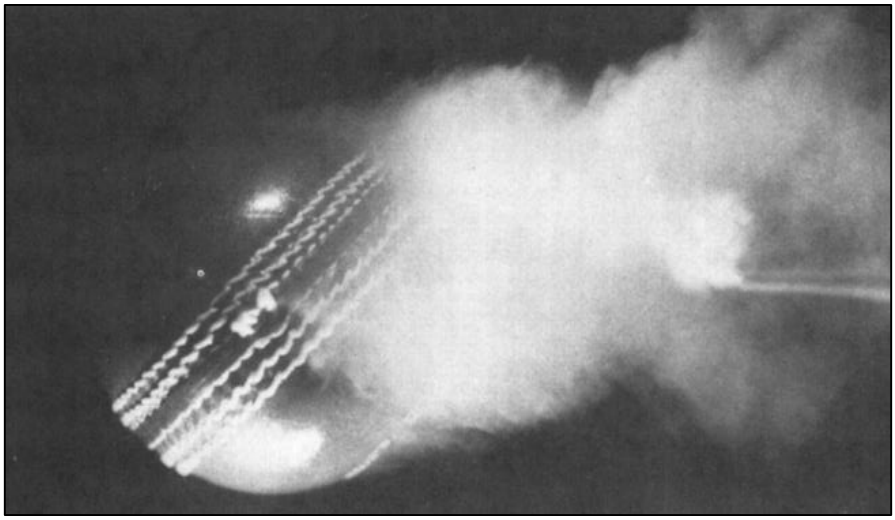

Figure 6 – Asymmetric location of seam on cricket ball resulting in "swing" during pitch (Mehta 2000)

Recall that the reason the "swing" occurs in Figure 6 is because the seam transitions the boundary layer to turbulent while the other remains laminar. For the opposite side to remain laminar, the ball must be traveling in its subcritical regime. What, then, occurs when a ball is pitched in the same configuration as Figure 6, but at a speed that puts it in

the supercritical regime of flight? As described relatively recently by Mehta (Mehta 2014), as the laminar, non-seam side undergoes transition due to increased Reynolds number, the boundary layer separation asymmetry hits a point where it no longer exists. Then, as the Reynolds number is increased beyond the zero-side-force point, the transition point on both sides will continue to move upstream. In this case, the transition point on the two sides is the same, but the turbulent boundary layer on the seam side has to negotiate the seam. The seam has a detrimental effect on the boundary layer and thickens it, making it separate earlier than it would have otherwise. This sets up a reverse wake deflection and results in a "Reverse Swing" motion of the pitch. Figure 7 depicts this case for a cricket ball in the supercritical flow regime.

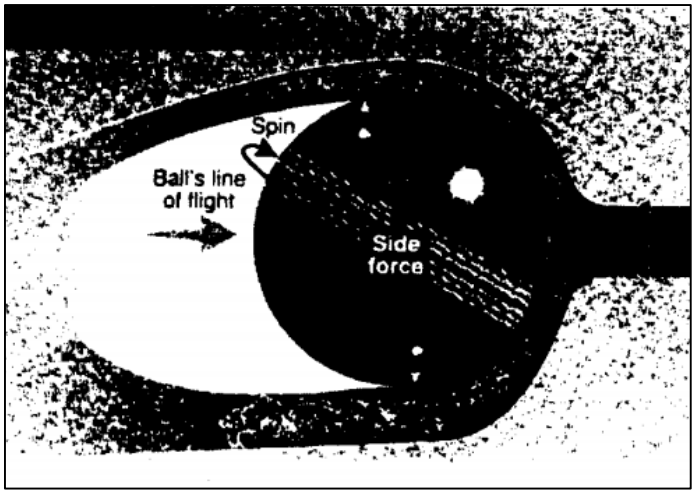

Figure 7 – Flow over cricket ball in "reverse swing" (Mehta 2014)

The interaction of boundary layers and asymmetric seams on a sports ball can produce a net force in the direction of the seam, no net force at all, or a net force in the opposite direction of the seams. The force is a function of the flow regime that the ball is in. This effect can quickly be related to scuffing on a baseball. A sports-ball seam affects the flow in a similar way as surface roughness does. Figure 8 shows how grit covering a sphere's lower half induces turbulent flow earlier than the smooth half and produces a deflected wake. Note that the case depicted in Figure 8 is clearly in the subcritical regime since the side without the roughness is separating earlier than the side with the roughness.

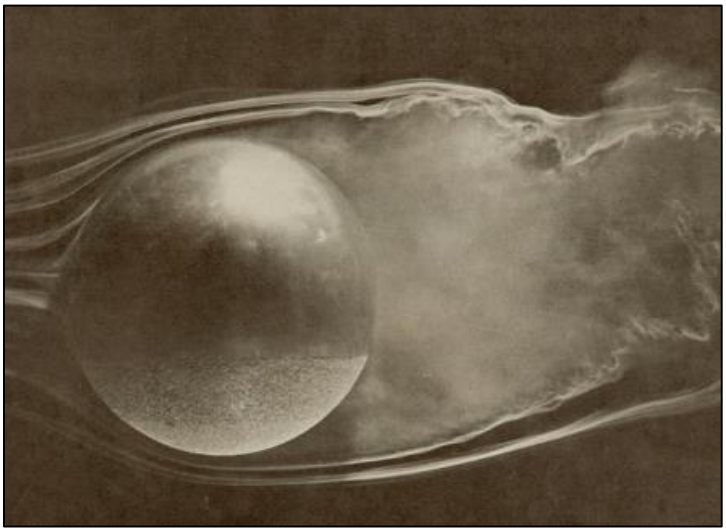

Figure 8 – Smooth sphere with grit on its lower half to create asymmetric separation points (Brown 1971)

Mehta showed that surface roughness can have a similar effect as a seam by creating "reverse swing" on a cricket ball. This again promotes the similarity between seams and surface roughness at affecting flow around a sphere. Figure 9

shows the effect that an old (roughed up) cricket ball has on generated swing force. The rougher the ball is, the earlier it reaches its critical Reynolds number and the more negative its reverse swing will become for a given velocity. Note that "reverse swing" is indicated by a negative force in Figure 9, and quarter seams essentially mean a rougher surface for the cricket ball.

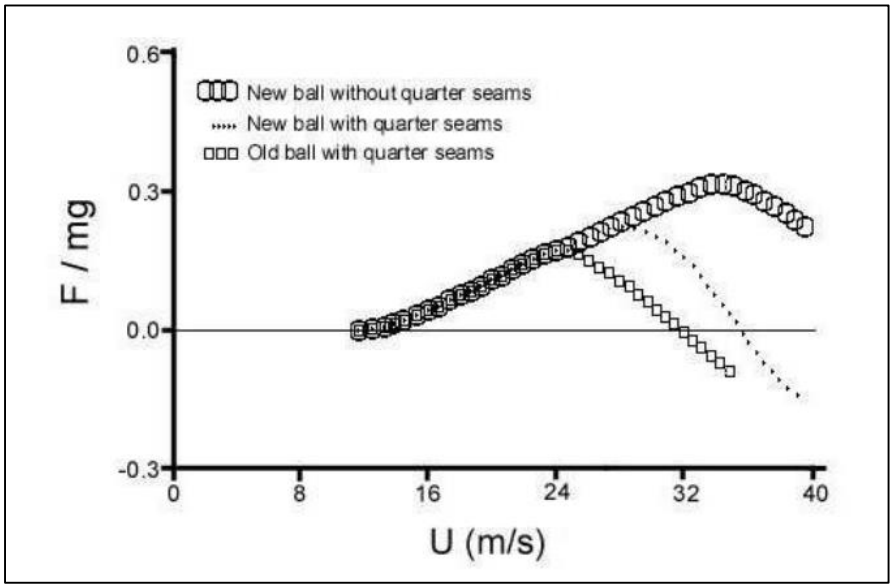

Figure 9 – Effect of surface roughness on normalized side force of cricket ball (Mehta 2014)

Mehta coins the term "Contrast Swing" for cricket balls in his paper. A schematic of this swing due to roughness is shown in Figure 10.

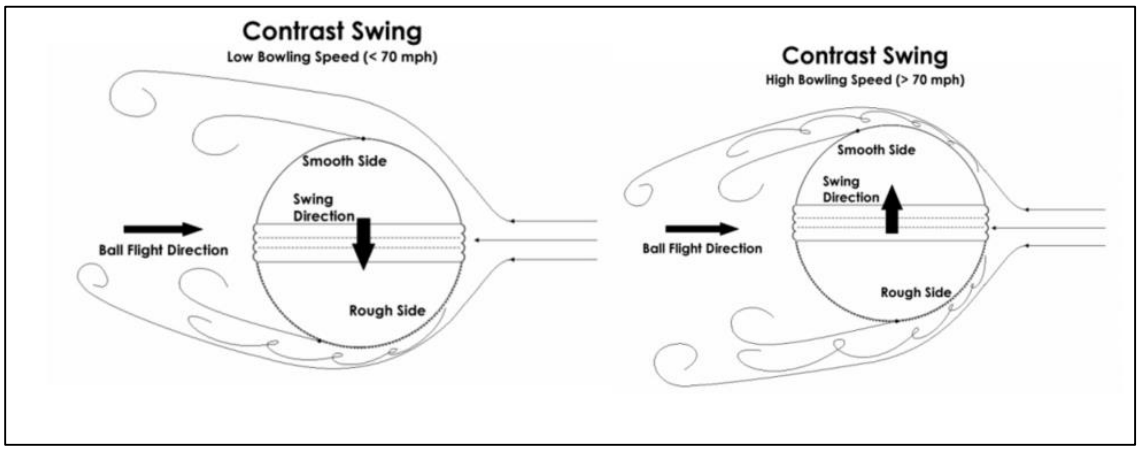

Figure 10 – "Contrast Swing" for cricket balls due to surface roughness (Mehta 2014)

In Part II of this paper, a theory is developed to predict the amount of side force that an asymmetrically rough sphere will experience as a function of Reynolds number. The results are then compared to these data on cricket balls.

II. Theoretical Model for Side Force of Asymmetrically Rough Spheres

The test results from Mehta for side force on cricket balls as a function of Reynolds number are understood quite well qualitatively, but there has been no way to quantitatively predict the magnitude of side force that an asymmetrically rough sphere will experience in a flow. For this reason, a theoretical model for side force as a function of Reynolds number was developed and is presented here.

Inspiration for the theory came from the thought-provoking figure below. Figure 11 depicts the characteristics of flow around a cricket ball with a seam angle of 15 degrees to the free-stream. The flow visualization was generated by injecting heat into the separated flow behind the ball and using thermal imaging to observe where the recirculating flow would creep up to. The limit of the red "hot" areas represents the separation point on the cricket ball.

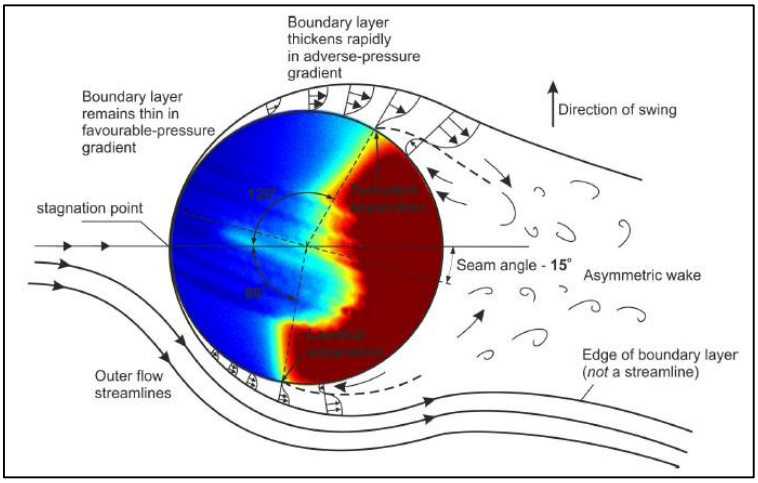

Figure 11 - Thermal image depicting separation point of flow over cricket ball with asymmetric seam (Scobie et al. *2014)*

The image shows that the flow appears to act in a very similar way to a ball with a symmetric separation point of 100 degrees (the average of 80 and 120) but at an angle of 20 degrees (half of the difference of 120 and 80) of to the free-stream. This inspired the following equation to be proposed as a model of side force on an asymmetrically rough sphere:

$$\boxed{C_Y = \sin\left(\frac{\Delta\phi_s}{2}\right) C_{D_{\phi_s avg}}} \quad \textbf{(1)}$$

$$where:$$

$$\Delta\phi_s = \phi_{s_1} - \phi_{s_1}$$

$$C_{D_{\phi_s avg}} = C_D\left(\frac{\phi_{s_1} + \phi_{s_1}}{2}\right)$$

$$\phi_{s_i} = separation\ point\ on\ side\ i$$

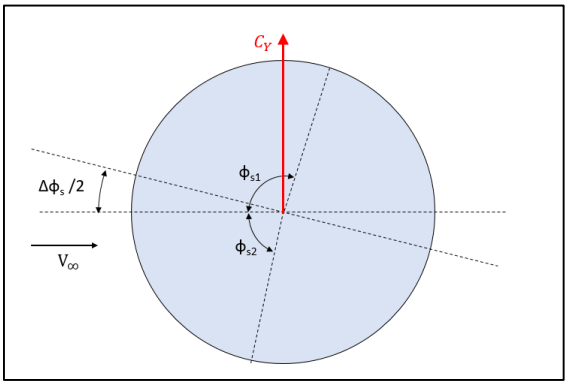

Figure 12 - Depiction of symbols used in Eq. 1

In addition to Equation 1, it is proposed that, to a large degree, the C_D of a sphere within the range near its critical Reynolds number should be a relatively simple function of ϕ_s. This idea has its origins in the data gathered by Dr. Elmar Achenbach (Achenbach 1974). In his paper, relationships between a sphere's surface roughness and its drag coefficient and ϕ_s are presented based on wind tunnel test data. Figure 13 and Figure 14 display these data.

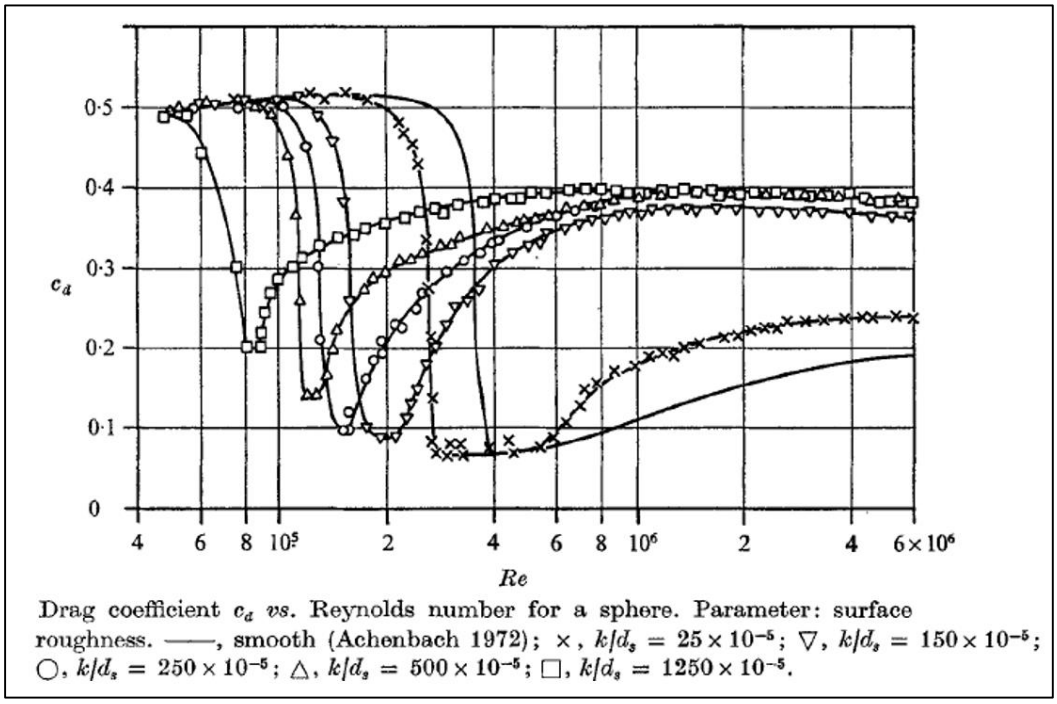

Figure 13 – (Achenbach 1974) Drag coefficient of sphere as a function of Reynolds number and surface roughness. Note surface roughness here is based off of spherical glass ball grit diameter. Corrected $k/d_{eff} = k/d_s * 0.55$. (Achenbach 1971)

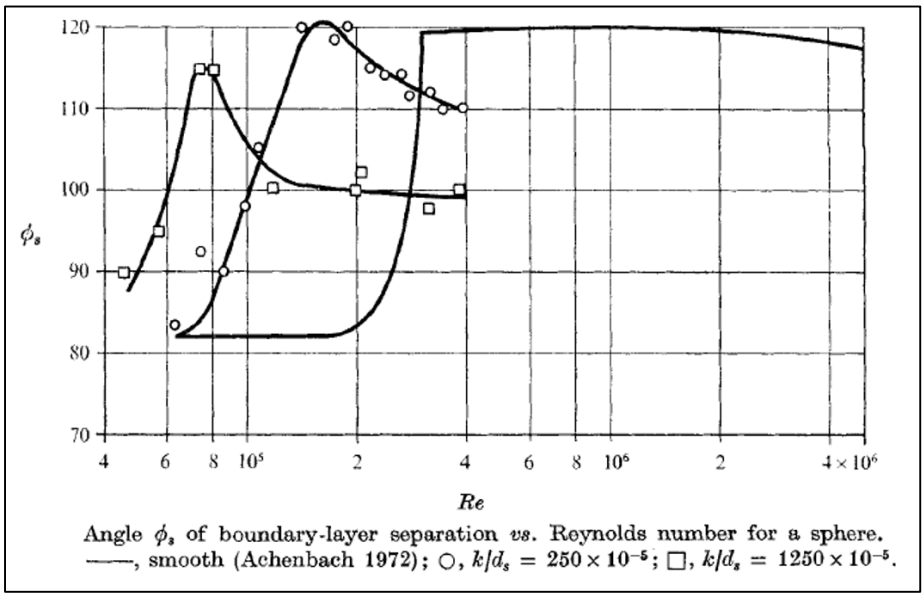

Figure 14 – (Achenbach 1974) Angle of separation as a function of Reynolds number and surface roughness. Note surface roughness is again based off of spherical glass ball grit diameter. (Achenbach 1974)

As noted by Achenbach himself, the C_D plots looks to be nearly the inverse of the ϕ_s plots. When looked at closely, it appears that C_D as a function of $\sin(\phi_s)$ can be estimated quite reasonably as a linear function in the subcritical regime and a second order function in the supercritical regime. It makes sense that slightly different relationships

between separation points and drag would occur before and after the critical Reynolds numbers because in once case the boundary layer is laminar and in the other it is turbulent. Figure 15 shows the data points collected by Achenbach and the simple best-fit-lines used to predict C_D as a function of ϕ_s. They are far from perfect, but are simple enough to capture the general trends in a sphere's drag coefficient quite well.

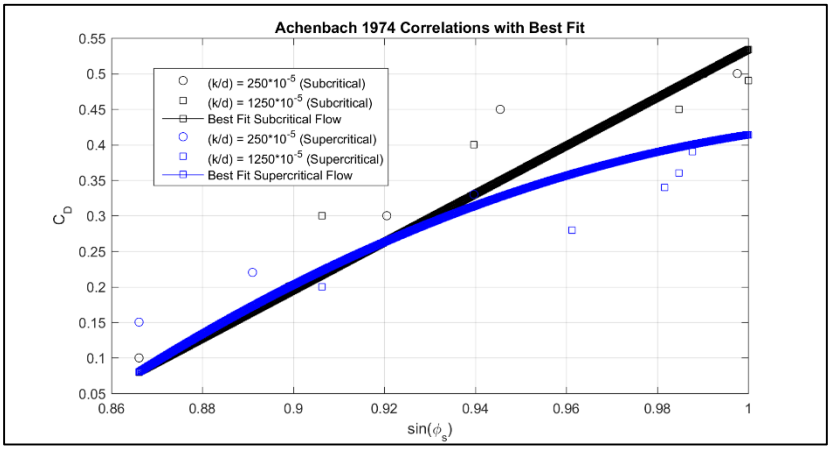

Figure 15 – Linear correlations used to predict C_D as a function of ϕ_s with Achenbach (1974) data included

The equations used for C_D as a function of ϕ_s are shown below (corresponding to heavy lines in Figure 15):

$$C_{D_{subcritical}} = 3.388 \sin\phi_s - 2.854 \quad (2)$$
$$C_{D_{supercritical}} = -11.198 \sin^2\phi_s + 23.388 \sin\phi_s - 11.776$$

Using the process documented in Appendix A, ϕ_s was parameterized as a piecewise function of Reynolds number and surface roughness. As a result, the ϕ_s curves given by Achenbach in Figure 14 can be created for any given surface roughness (within reasonable roughness ranges). Figure 16 and Figure 17 show the predicted results for ϕ_s and C_D, respectively. Note that the C_D was generated using the relationships in Equation 2.

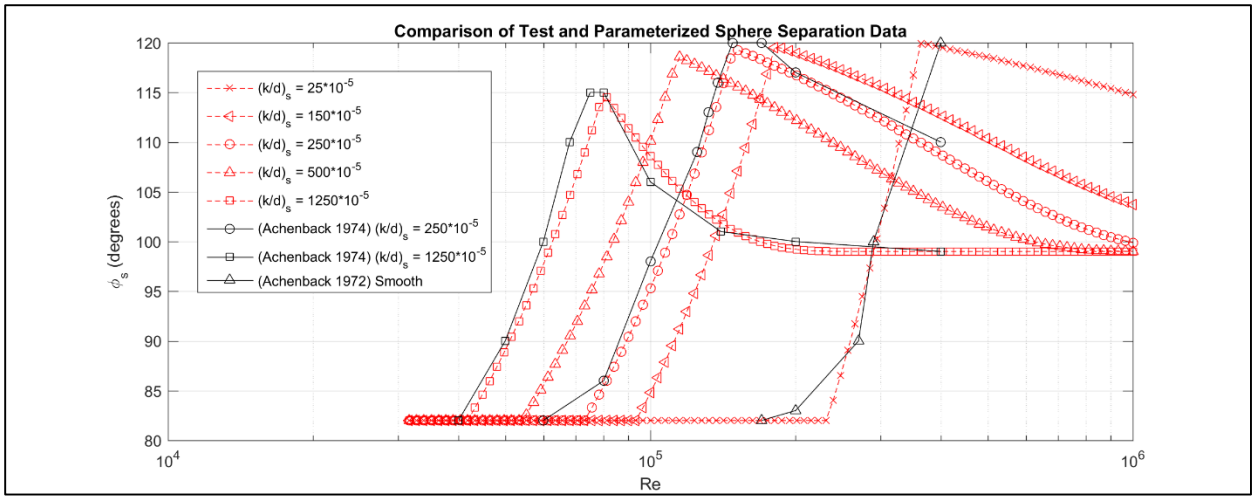

Figure 16 – Piecewise parameterization results for ϕ_s as a function of Reynolds number and comparison to Achenbach (1974) data

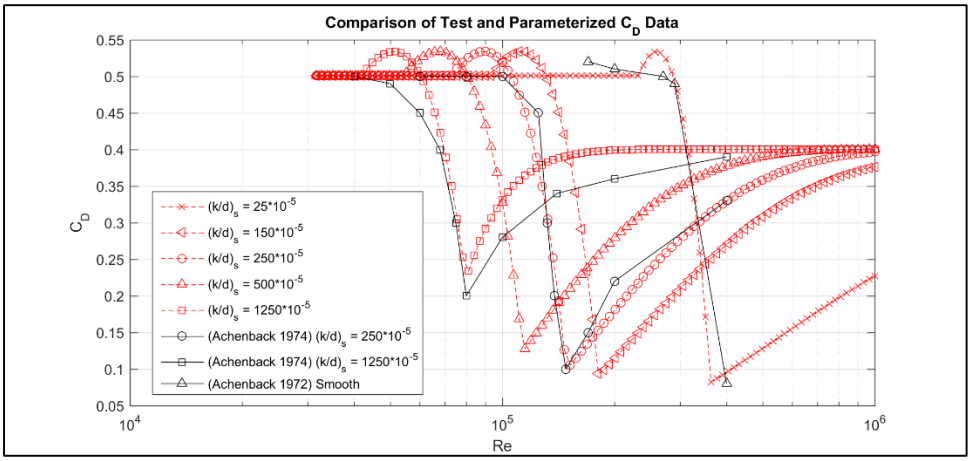

Figure 17 – C_D as a function of Re using the piecewise parameterized ϕ_s depicted in Figure 16 and linear relationships in Eq. 2

Figure 17 shows that the model seems to work quite well at predicting ϕ_s as a function of $(k/d)_s$ up to at least about $(k/d)_s = 1250*10^5$. In addition, Figure 17 shows that the linear relationships in Equation 2 predict C_D quite well. The C_D predictions are a bit inaccurate in the supercritical flow regime for high roughness spheres, but overall they are not terrible considering such a simple relationship was used.

With a methodology to predict ϕ_s and C_D as a function of surface roughness and Reynolds number, predictions can be calculated for the side force that an asymmetrically rough sphere will experience as a function of velocity. Up to this point, the two sides of the sphere have been analyzed independently. In reality, the two sides will affect each other because they are comparatively close to each other in subsonic flow. Perhaps the largest way they will affect each other is in determining the flow's pressure in the separated wake (base pressure). The base pressure is largely constant and therefore must be the pressure behind each side's separation point. Interestingly, this sets up a bit of an unstable flow pattern for an asymmetrically rough sphere. When the rough side transitions to turbulent flow first, the base pressure will want to increase. This will tend to aggravate the smooth side's separation due to adverse pressure gradients and the flow will exhibit a bit of hysteresis. Once the smooth side transitions, the rough side will see a higher adverse pressure gradient and should tend to separate earlier since it is now post-critical Reynolds number and in a retreating condition.

These interactions are complex and beyond the scope of the simplified model set up in this paper. However, in order to accurately capture correct post-critical Reynolds number characteristics, a simple modification can be made to the rough side of the sphere's separation point. The rough side of the sphere's separation point can be modeled as:

$$\boldsymbol{\phi_{s_{rough}} = max\left(82, \phi_{s_{rough}} - \left(\phi_{s_{smooth}} - 82\right)\right)} \quad \textbf{(3)}$$

The simple modification effectively moves the rough side's separation forward due to the increased base pressure from the opposite side. It assumes that the rough side of the sphere is sufficiently more-rough than the smooth side. If the two sides are very similar in roughness, it is probably better not to apply this modification.

The cricket ball configurations from Figure 9 were modeled to see how closely the described method would predict side force on a cricket ball with an angled seam. Based on the inflection points of the curves in Figure 9, the $(k/d)_{eff}$ of the different cricket ball surfaces were selected and presented in Table 1. Note from Achenbach, $(k/d)_{eff}$ is equal to $(k/d)_s * 0.55$. Achenbach used small glass spheres to create roughness, and their effective roughness was only about 0.55 of their diameter based on other testing he performed.

Table 1 – Equivalent $(k/d)_{eff}$ used to model cricket balls based on inflection points of Figure 9

Configuration	$(k/d)_{eff} * 10^5$
Old ball with quarter seams	53
New ball with quarter seams	38
New ball without quarter seams	25
All balls on seam side	200

The predicted normalized side force as a function of velocity is shown in Figure 18. The test results from Mehta (2014) are also shown for comparison.

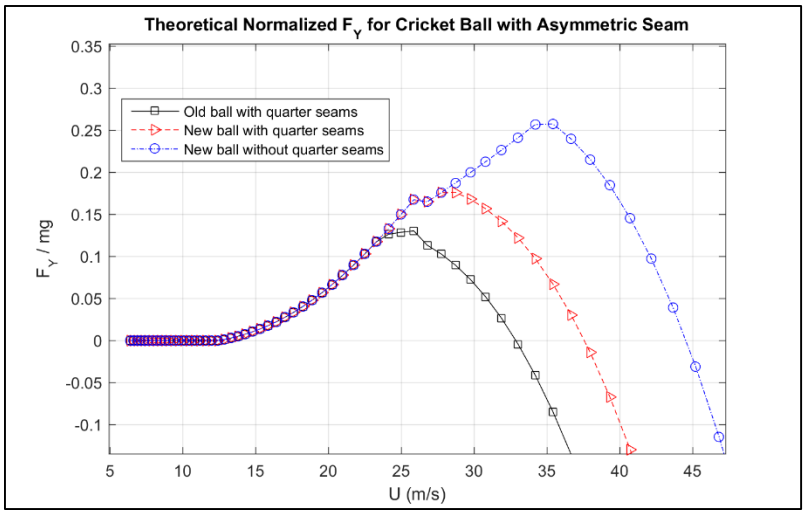

(a)

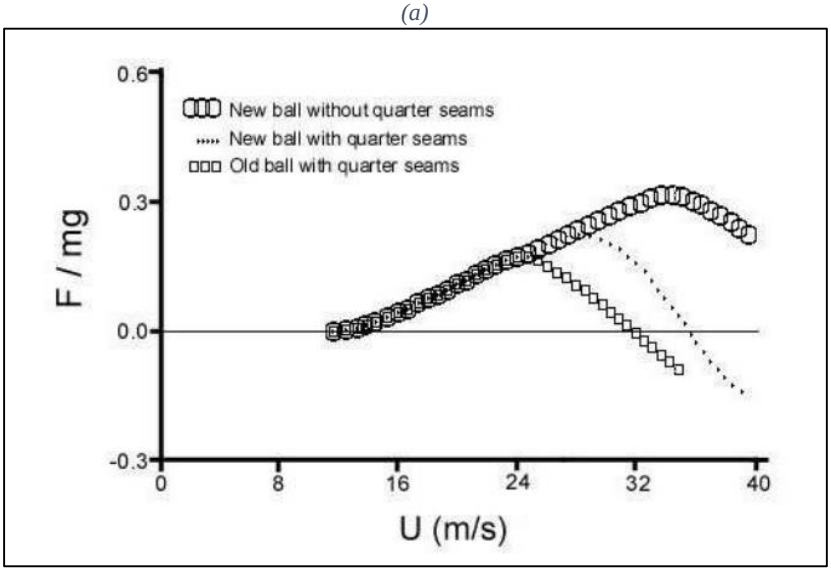

(b)

Figure 18 – Theoretical side force as a function of velocity (a) and measured side force as a function of velocity (Mehta 2014)

Figure 18 shows that the model predicts the side force of a cricket ball quite well. This gives a good indication that the model in Equation 1 works well at predicting side force for asymmetrically rough spheres. One thing to note is that the force magnitudes are a little under-predicted in the model relative to the test data. The model predicts about 15 to 20 percent less side force than the test data show.

An interesting way to explain the root-cause of the results in Figure 18 is to look at the separation points of the different configurations. Figure 19 shows the separation points of the modeled cricket balls. Note that the

modification from Equation 3 is not applied to the rough (seam) side in the figure because it would adjust the rough side's separation point differently for each of the 3 scenarios.

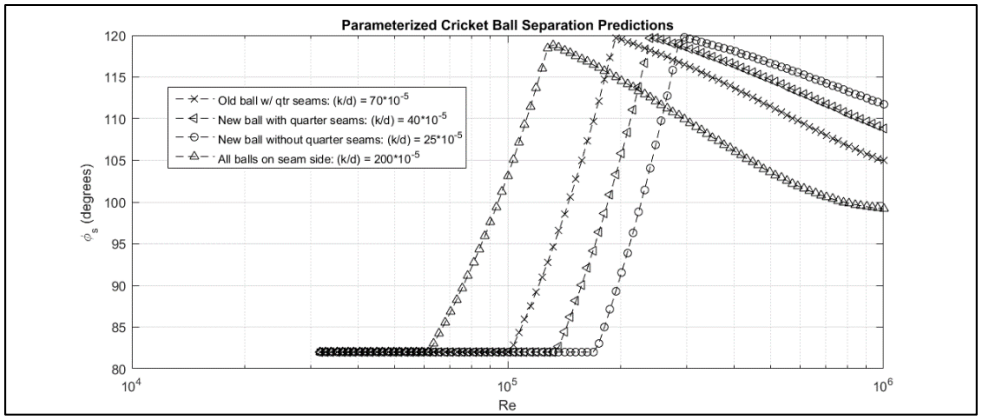

Figure 19 – Predicted cricket ball separation points as function of Re

Figure 19 shows that the seam side trips the flow at lower speeds and causes the positive side force. However, at higher speeds, the seam side begins to separate earlier and the non-seam side begins to stay attached longer. When the two curves cross, the side force is zero. Beyond that point, the side force enters the "reverse swing" region and the side force is negative. This model aligns with the qualitative description of the physics of reverse swing in Part I, but here a numerical prediction for side force can be reached based off of parameterized curves.

An interesting plot from the model is the side force coefficient of the cricket balls at high speeds. Figure 20 shows what the model predicts at high speeds. The figure shows that there is a limit to the side force coefficient that the model can predict on the ball. Depending on the combination of roughnesses, the maximum magnitude of side force coefficients is about ± 0.15. Of course, this is just a theoretical limit produced by the simple model. In reality, the model tends to under-predict side force magnitudes so the limit is actually wider than 0.15, but there should be an approximate limit on side force for an asymmetrically rough sphere.

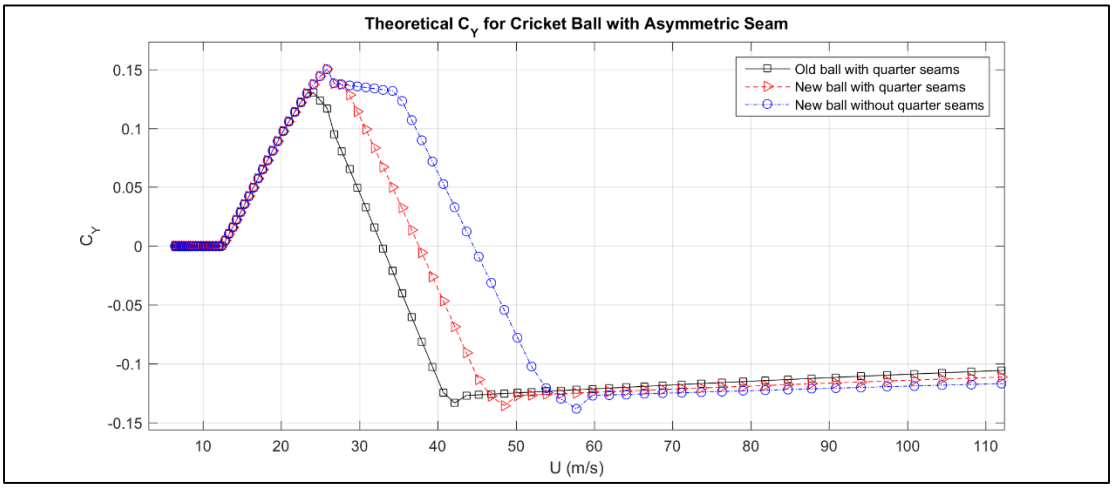

Figure 20 – Predicted normalized side force on asymmetric cricket ball at high speeds.

III. Wind Tunnel Testing of Asymmetrically Roughened Sphere and Baseball

A. Test Setup and Configuration

Two wind tunnel tests were performed at the University of Washington Kirsten Wind Tunnel to investigate the impacts of asymmetric scuffing and foreign object application on baseballs. The tunnel has a 10'x10'x12' test section, and is a dual-circuit return tunnel with 0.72% turbulence intensity. The first test was a learning experience and the data were considered too noisy to use. Only the second test's data are presented in this report. The test number was UW2139.

A sting-type mount was used with an ATI Mini-40-E Six-Axis Force/Torque transducer mounted inside of the tested spheres for minimum interference. The transducer was connected to an ATI sensor system used to record force and moment data. The sphere tested was designed with the SolidWorks CAD program and was 3D printed using a high-quality printer. The sting mounting equipment was welded and then machined on a 3-axis mill to achieve tight tolerances. The mount system with the bare sphere is shown in Figure 21.

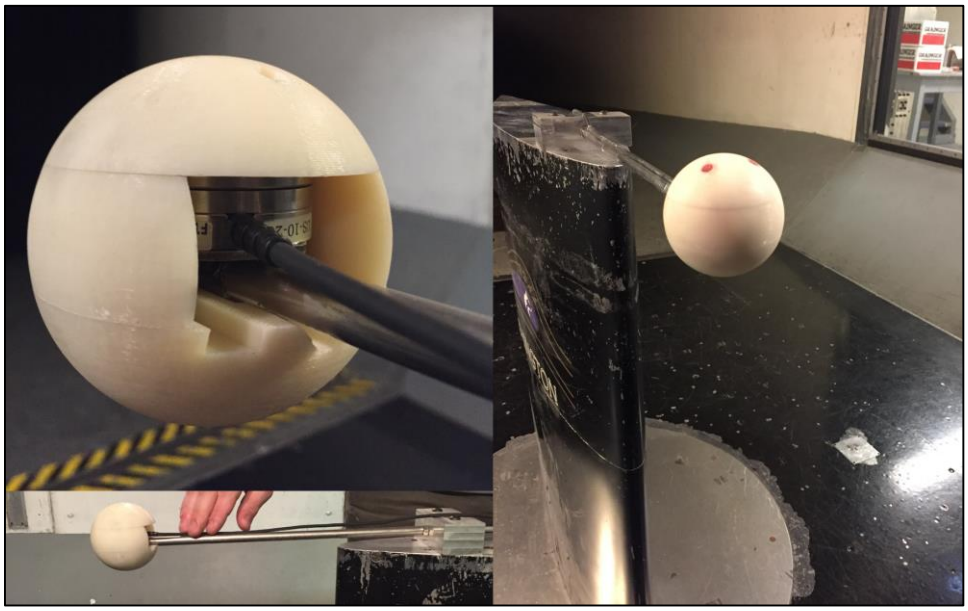

Figure 21 – 3D Printed sphere installed in Kirsten Wind Tunnel test section with internal balance

The balance was calibrated using known weights. There was a linear correlation between force and voltage coming from the channels of the transducer. There was a slight interaction between Y-Force and Z-Force in balance coordinates, so a linear balance interaction was applied to all data collected.

An official Major League Baseball was tested by removing the outer leather of a baseball by slitting it along its aft side, wrapping it around the 3D printed sphere (designed to be the exact size of a baseball core), and sewing the leather back together. A clay-wax mixture ("clax") was used to fill in the small gap in back of the baseball. This setup is shown in Figure 22.

Figure 22 – Test configuration for baseball with internally mounted balance on sting mount

B. Tunnel Calibration and Sphere Testing

The 3D printed sphere was tested in the wind tunnel to compare the its drag coefficient to the known drag coefficient of a sphere at its sub-critical Reynolds number of about 0.5. Figure 23 shows the drag coefficient of the 3D printed sphere as a function of Reynolds number. The pre-critical Reynolds number drag coefficient was measured to be about 0.47. This is a little less than 0.50, but is pretty close to the expected value and indicates high quality data. In addition, the scatter of the data in Figure 23 is quite minimal and indicates that the 5-second averaged test points were able to sufficiently capture trends in the data.

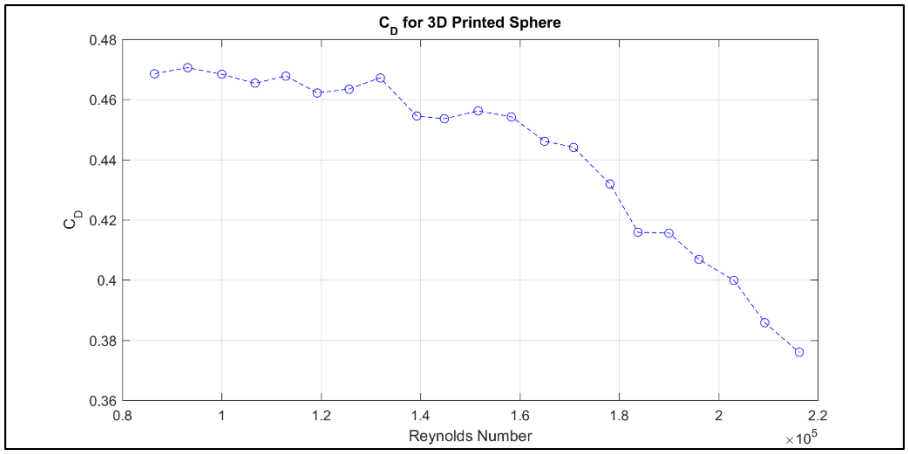

Figure 23 – C_D for smooth 3D printed sphere as a function of Reynolds Number

One side of the sphere was roughened by sanding it with 80-grit sandpaper. The side force relative to the baseline sphere is shown in Figure 24. It was observed that while testing at the Kirsten Wind Tunnel, the Reynolds number range that ϕ_s took to go from its furthest forward point to its furthest aft point was less wide than the Achenbach and Mehta data. This was possibly due to either the roughness patters or a bit higher turbulence levels in the flow of the tunnel tested at, although this is not known for sure. It would be interesting to see how the speed of transition in the Reynolds number domain is a function of turbulence or other factors. Nevertheless, a factor of 0.25 was applied to the $\Delta RE_{subcritical}$ parameter described in Appendix A for all theoretical predictions of data obtained at the Kirsten Wind Tunnel to better match test data. This trend was consistant across all tested configurations.

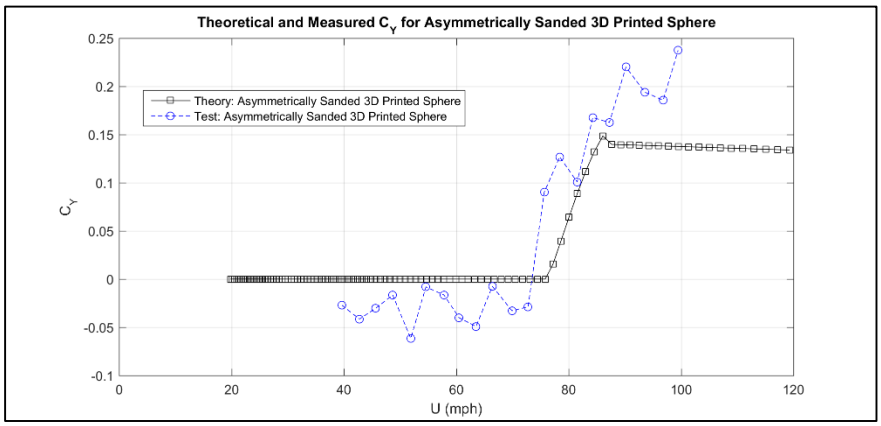

Figure 24 – Theoretical and measured C_Y for asymmetrically sanded 3D printed sphere

Figure 24 shows that the side force coefficient for the sanded ball was predicted decently well for the sanded sphere, but the magnitude of side force was under-predicted by a good margin. The model seems to do a better job at predicting general characteristics rather than exact magnitudes of side force.

C. Baseball testing

Figure 25 shows the theoretical and measured C_D and C_Y for an asymmetrically scuffed baseball. The scuffed baseball is shown in Figure 26.

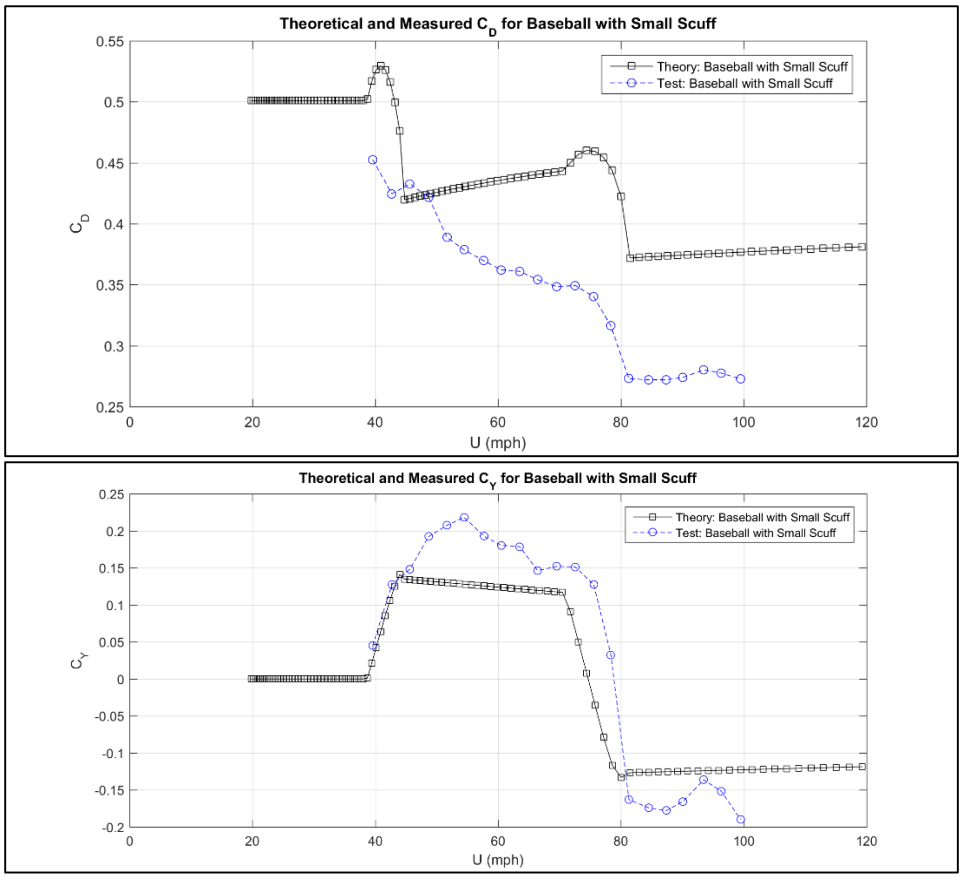

Figure 25 – Theoretical and Measured C_Y and C_D for asymmetrically scuffed baseball

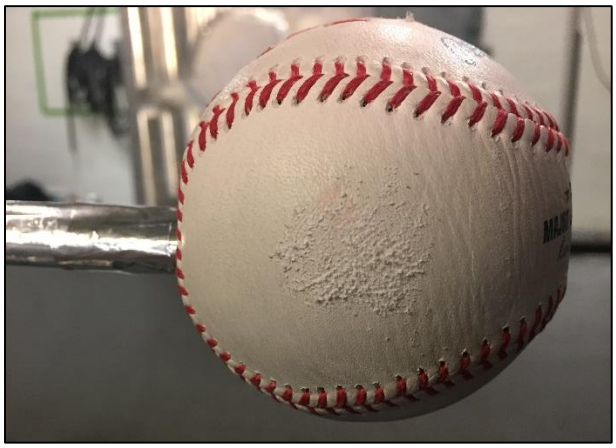

Figure 26 – "Scuffed" baseball (80-grit sandpaper used)

The C_Y plot in Figure 25 shows that the theoretical model for side force does a pretty good job at predicting the trends in side force. Although it slightly under-predicts the side force magnitude, a limit seems to exist on both the positive and negative side force coefficients. The theoretical C_D was found using Equation 4 which uses the cosine of the half differential separation angle (instead of its sine).

$$C_D = \cos\left(\frac{\Delta\phi_s}{2}\right) C_{D_{\phi_s avg}} \quad \textbf{(4)}$$

The drag prediction in Figure 25 is not perfect, but the testing does exhibit a 2-step pattern like the theory predicts. The first step is from the rough side transitioning to turbulent flow, and the second is from the smooth side transitioning.

A baseball was also tested with clax applied to its side. The clax was used to simulate pine-tar rubbed onto the side of the ball. This is a practice that more than a few pitchers and catchers have been accused of using to generate lateral movement in pitched baseballs. It was even observed during the 2015 World Series that the catcher was rubbing pine tar onto the baseball before the pitcher would receive it. Figure 27 shows the tested configuration, and Figure 28 shows the test results.

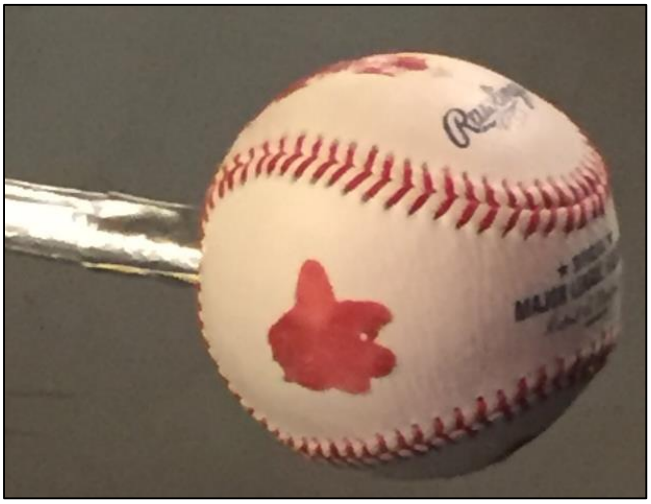

Figure 27 – "Clax" applied to simulate pine-tar application to side of baseball

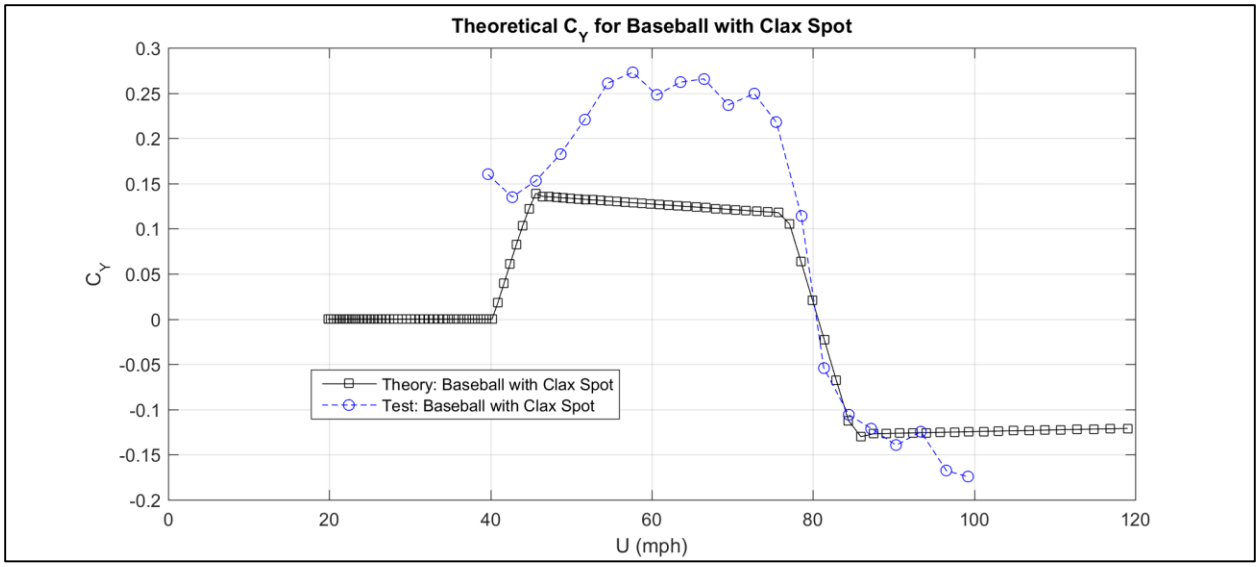

Figure 28 – Theoretical and Measured C_Y of baseball with "clax" applied to simulate pine-tar application

Figure 29 shows that something applied to the side of a baseball has nearly the same effect that a scuff does. In fact, at speeds below ~80 miles per hour, the clax actually created larger side force than the scuff. Again, the theory under-predicted side force magnitude, but predicted the trends quite well.

One last interesting configuration tested was a baseball with trip-dots applied to one side of a baseball. This configuration is more aerodynamically interesting than one that is applicable to simulate a pitched ball. Figure 29 shows the test configuration and Figure 30 shows the test data.

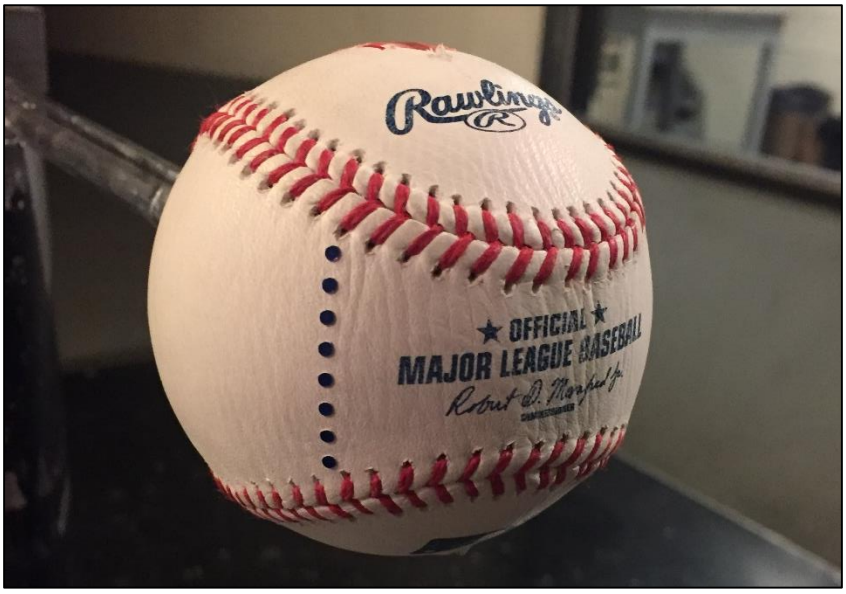

Figure 29 – Baseball with trip does applied to one side

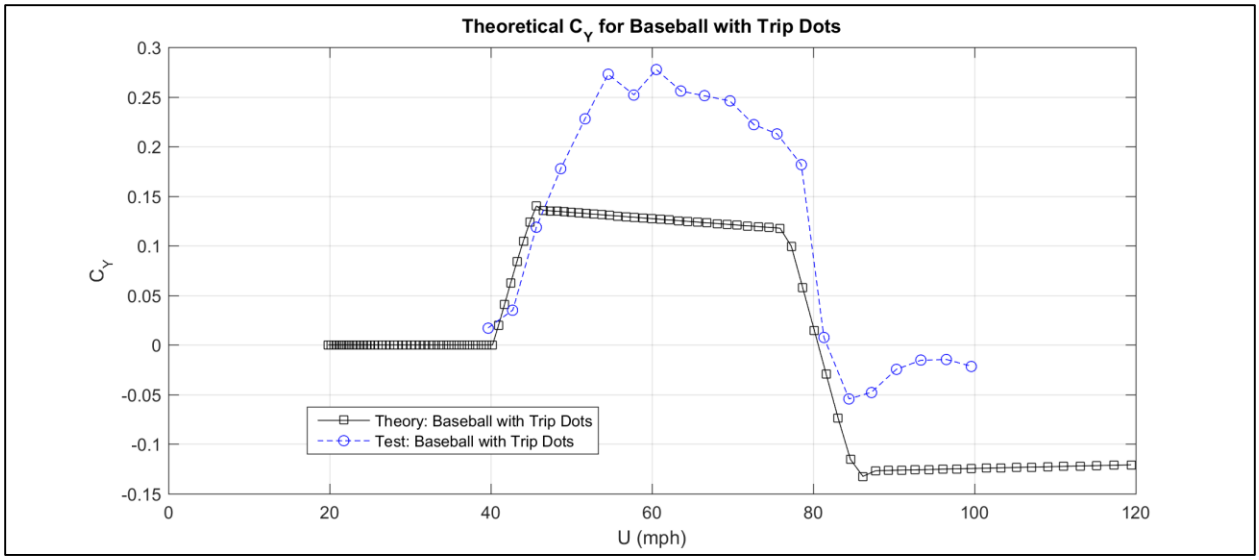

Figure 30 – Theoretical and Measured C_Y of baseball with trip dots applied to one side

Interestingly, the negative side force in Figure 30 saturates at a lower value than the theory predicts. This was investigated, and an interesting characteristic was found. If the trip dots are assumed to do a very good job at keeping the boundary layer attached post-critical Reynolds number, the modification in Equation 3 should be removed. Removing the modification results in the theoretical prediction shown in Figure 31.

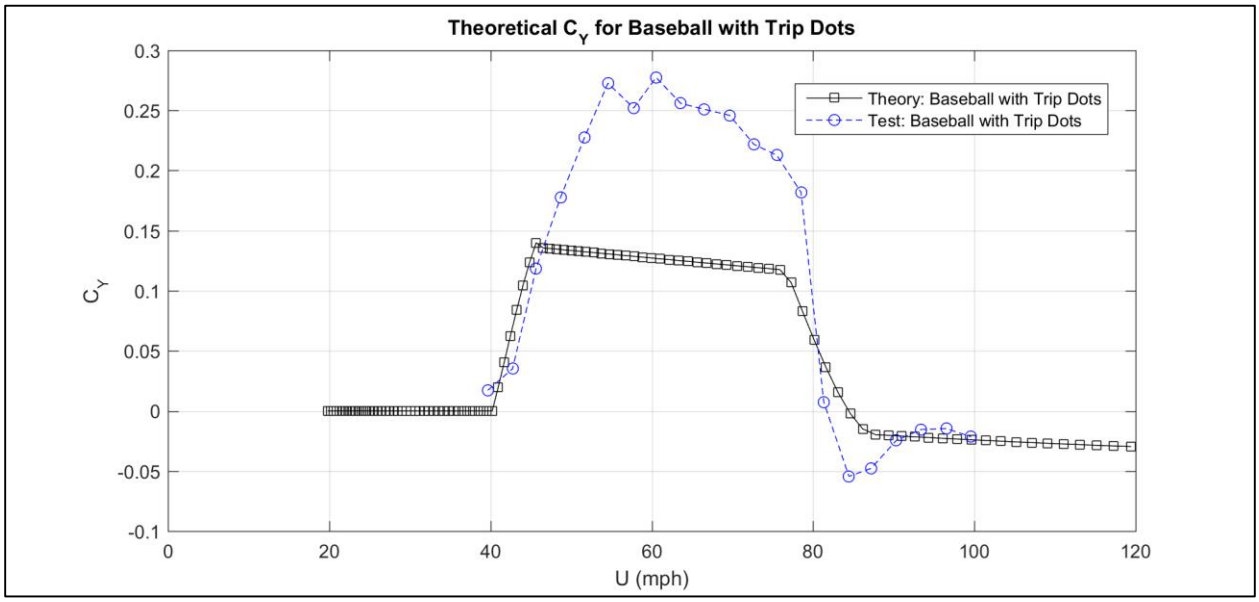

Figure 31 - Theoretical and Measured C_Y of baseball with trip dots applied to one side (No Eq. 3 applied to theoretical)

Figure 31 shows that if the trip dots are assumed to do a good job of keeping the flow attached on the rough side (as they are designed to do), the theoretical C_Y matches the test data almost perfectly once the smooth side reaches its critical Reynolds number.

IV. Dynamics of pitch with contrast curve

In Section III, it was concluded that a scuffed or altered baseball in about 95 mph airflow experiences a C_Y of about 0.15. However, the assumption of this force coefficient magnitude is that the effect of rotating seams is minimal. When a 2-seam fastball is actually thrown, the seams may have a stabilizing effect to the flow around the ball. If this stabilizing effect is assumed to result in a 1/3 reduction in produced side force, a C_Y of about 0.10 would be produced from a scuffed or altered baseball. If this force were constant during the pitch's flight to home plate, how much would the pitch move horizontally? Using basic Newtonian physics and neglecting drag, Figure 32 shows how the flight path of a scuffed baseball would change.

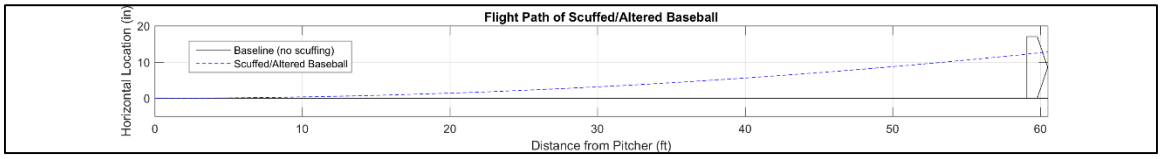

Figure 32 – Flight path of scuffed/altered baseball with C_Y of 0.10

Figure 32 shows that a scuff on a baseball can affect its flight path to a large degree. Home plate is shown (to scale) on the right side of the plot. For a C_Y of 0.10, a baseball will move almost an entire strike-zone width. It should be noted that for a given C_Y, horizontal displacement is not a function of pitch speed. This is because the acceleration is proportional to V^2 and the square of flight time is proportional to $1/V^2$, meaning that for a given C_Y, the flight path is not a function of velocity (if drag is neglected).

For a batter, the pitch in Figure 32 would be very difficult to hit. It would be impossible to see the scuffing on a spinning baseball and anticipate the horizontal movement of the ball. A batter could be easily fooled and swing at a pitch that looks like it will be a strike but breaks away an additional 13 inches. To give an idea of the sensitivity of pitch movement as a function of side force coefficient, Figure 33 was created.

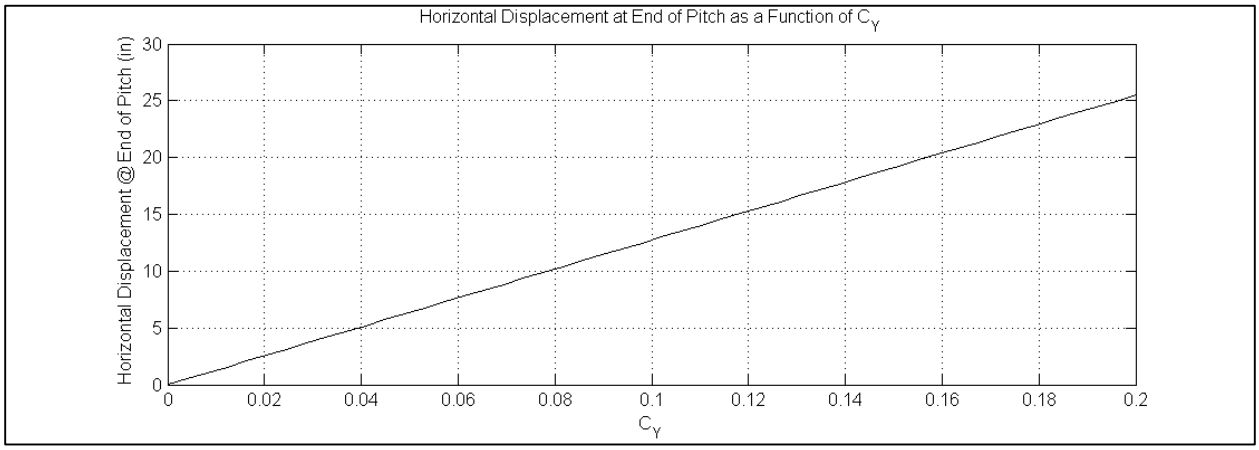

Figure 33 – Horizontal displacement at end of pitch as a function of C_Y

Even a few inches of movement can cause issues for batters. Figure 33 shows that even if a baseball were barely scuffed and experienced a C_Y of 0.04, it would move about 5 inches horizontally during its flight to home plate.

V. Conclusions and Lessons Learned

The model developed in this paper to predict side force on a sphere as a function of asymmetric surface roughness and Reynolds number predicts side force reasonably well for the sports balls analyzed. It is not perfect and the actual magnitude of the side force is generally greater than the model predicts. Considering the complex flow physics of separated flow around an asymmetrically rough sphere with seams, the model seems to do a decent job. To fully understand any sphere's aerodynamic behavior, wind tunnel testing (or some other form of aerodynamic testing) is definitely needed, but rough predictions can be made with the model if critical Reynolds numbers or equivalent surfaces roughnesses are known. It would be interesting to apply the model to a rotating sphere and see if Magnus force could be predicted.

The frequent replacement of Major League baseballs is well warranted based on the wind tunnel data collected. A small scuff or substance applied to the side of a ball can produce significant side force at Major League pitch speeds. Data indicate that a ball with pine tar on its side could move anywhere between 5 and 15 inches depending on its speed and the effect of rotating seams.

The concept of side force reversal at the smooth side's critical Reynolds number was predicted and observed during the baseball testing. This has interesting implications on many past data collected on baseballs. In fact, even classic papers like Watts and Sawyer "Aerodynamics of a Knuckleball" (Watts, Sawyer 1975) overlook the sensitivity of Reynolds number on the lateral force of a seam tripping the flow. They would have measured the opposite lateral force had they tested at 90 miles per hour instead of about 46 miles per hour.

One implication of this study is how drastic the effect of asymmetric seams can be. Anecdotally, I have observed 2-seam fastballs "tail" (or move horizontally) quite large distances. This was probably occurring because the spin axis was slightly tilted in the direction of travel, creating an asymmetric seam pattern. This type of pitch is shown in Figure 34. A pitcher could use the legal "Contrast Curve" pitch depicted to his advantage.

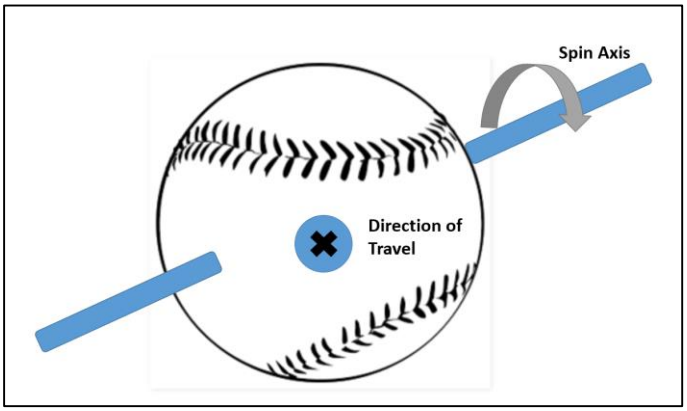

Figure 34 – Legal "Contrast Curve" type pitch

During wind tunnel testing a few lessons were learned. Firstly, sphere aerodynamics are highly sensitive to surface finish and much care needs to be taken to correctly align any tested configuration with the wind. In addition, having a balance inside of the sphere being tested produces high-quality data that has minimal noise. If a balance is external to the model, it must be kept out of the wind or else data will be too noisy to interpret.

Overall, this project has been a fun AA290 project at Stanford. There is definitely more that could be done to improve the side force model's predictions. If many different combinations of asymmetrically rough spheres were tested, perhaps the model could be better calibrated.

Thank you to Rabi Mehta for suggesting looking at side force due to scuffing on baseballs and for his guidance in testing methods. Also thank you to the Kirsten Wind Tunnel staff and crew for all of the help building and testing the models.

Appendix A – Parameterization of ϕ_s as a function of Reynolds number

A theory is developed to parameterize the curves of ϕ_s as a function of Reynolds number and surface roughness from Achenbach (1974). The available data is referenced below:

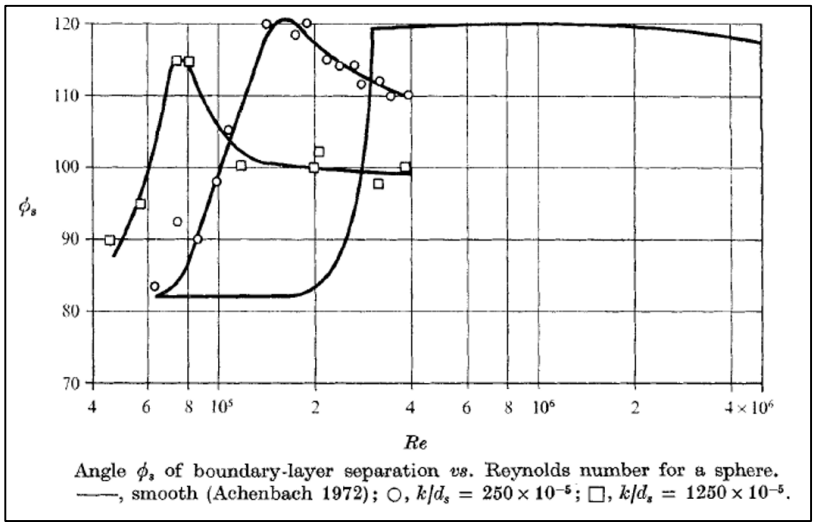

Figure A 1 – (Achenbach 1974) Wind tunnel test data for ϕ_s as a function of Reynolds number and surface roughness

In general, the ϕ_s curves for a given roughness can be characterized given 3 points in the domain. These points are depicted in Figure A 2 below.

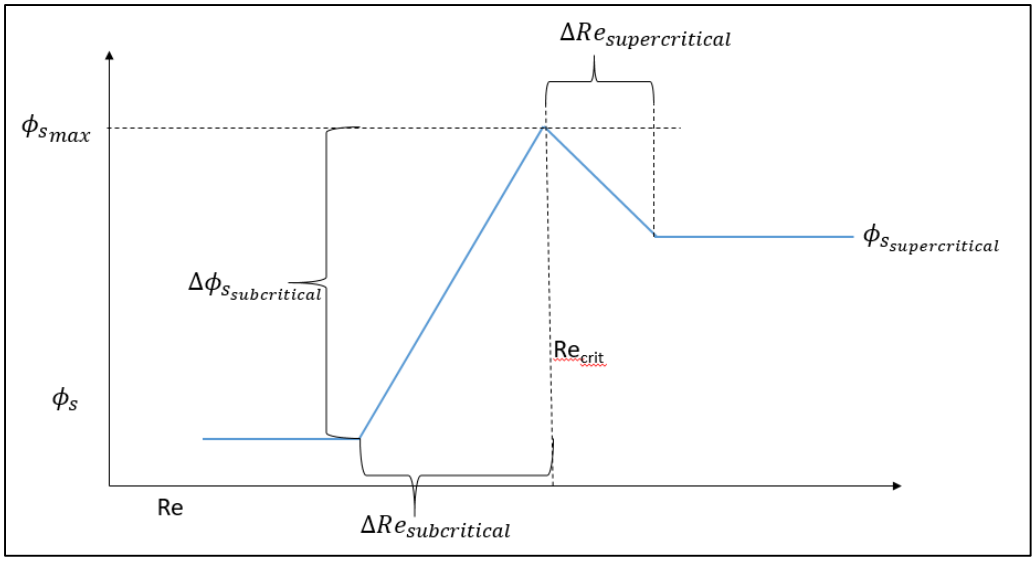

Figure A 2 – Parameterized ϕ_s curve

Using the data from Achenbach's paper, the different parameters depicted in Figure A2 were found as functions of effective surface roughness.

In his paper, Achenbach (1974) plots the critical Reynolds number as a function of surface roughness. Upon further inspection, the critical Reynolds number can be very accurately represented as a power law:

$$Re_{critical} = 11700 * \left(\frac{k}{d}\right)_{eff}^{-0.386}$$

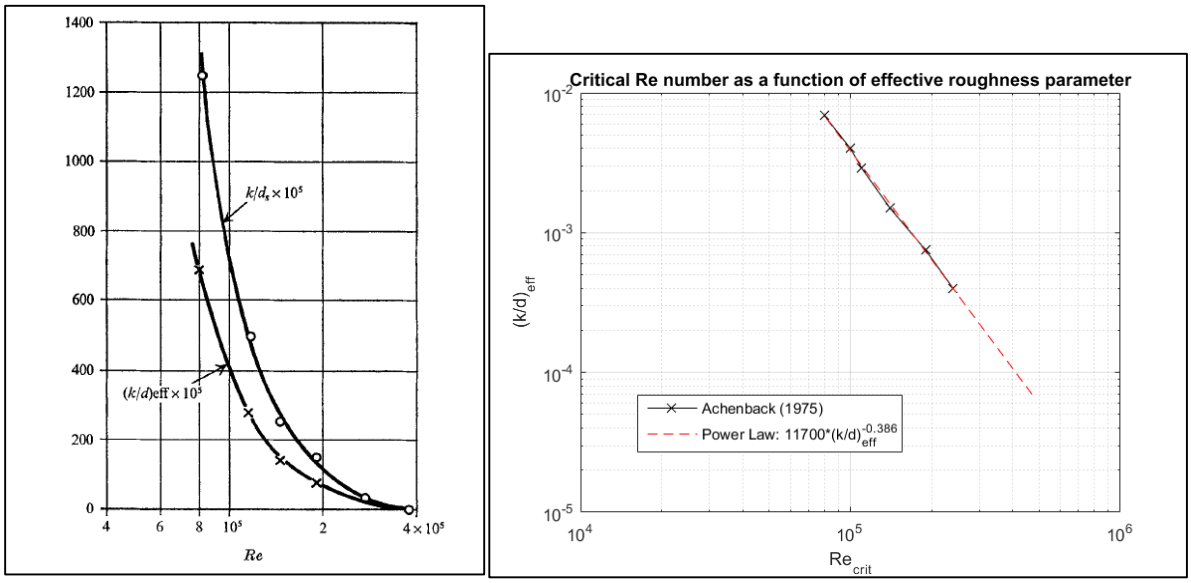

Figure A 3 – (Achenbach 1974) Critical Reynolds number as a function of $(k/d)_s$ and $(k/d)_{eff}$, with corresponding log-log power law representation on right

$\phi_{s_{max}}$ was approximated by a second order fit based on Achenbach's data. The data and corresponding equation are shown in Figure A 4.

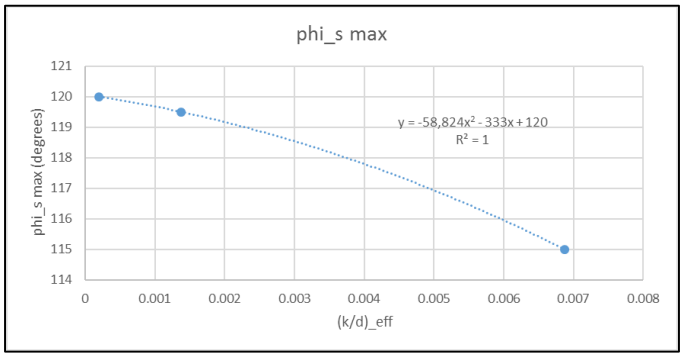

Figure A 4 - $\phi_{s_{max}}$ as a function of k/d_{eff}

$\Delta\phi_{s_{subcritical}}$ is simple to represent because the subcritical ϕ_s is consistently ~82 degrees. Thus:

$$\Delta\phi_{s_{subcritical}} = \phi_{s_{max}} - 82$$

$\Delta Re_{subcritical}$ can be modeled quite well with a logarithmic fit as shown in Figure A 5.

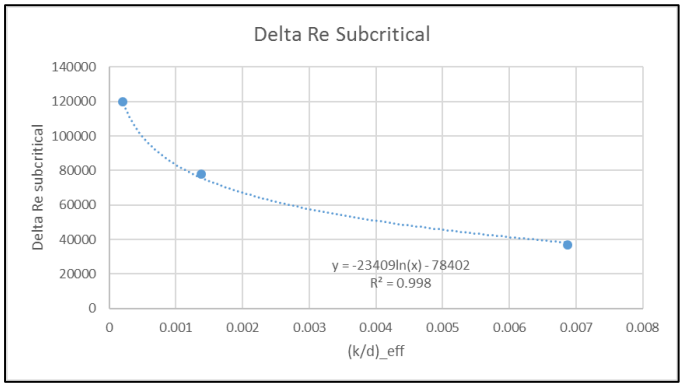

Figure A 5 - $\Delta Re_{subcritical}$ as a function of k/d_{eff}

$\Delta Re_{supercritical}$ can also be modeled quite well with a logarithmic fit as shown in Figure A 6.

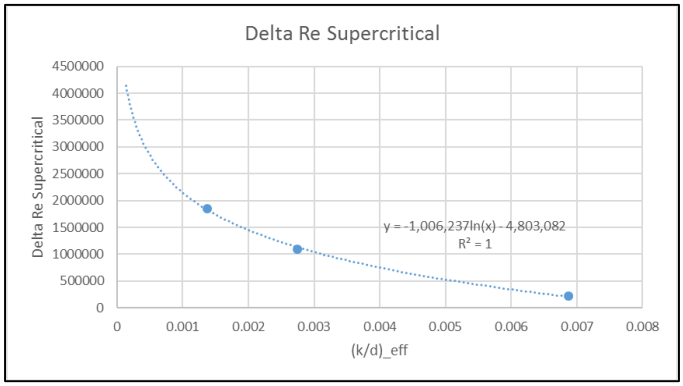

Figure A 6 - $\Delta Re_{supercritical}$ as a function of k/d_{eff}

$\phi_{s_{supercritical}}$ proved to be a bit difficult to parameterize. It works best when $\phi_{s_{supercritical}}$ is modeled with a logarithmic fit as shown in Figure A 7. However, based off of observations, it appeared that the separation point did not continue past $\sim\phi_s = 99\ degrees$. Thus, the following piecewise equation was used to predict $\phi_{s_{supercritical}}$:

$$\phi_{s_{supercritical}} = \max\left(99, -5.148\ ln\left(\left(\frac{k}{d}\right)_{eff}\right) + 65.1\right)$$

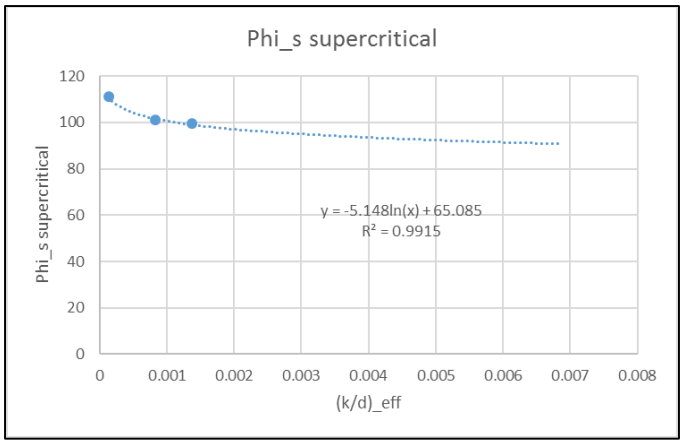

Figure A 7 - $\phi_{s_{supercritical}}$ as a function of k/d_{eff}

With these equations, the three points of the simplified ϕ_s curve in Figure A 2 can be generated. In between the first two points, a linear interpolation was used. In between the second two points, a 5th order interpolation was used to fit the shape of the plots better. This fit the data much better than a linear interpolation. The interpolation between Re_{crit} & $\left(Re_{crit} + \Delta Re_{supercritical}\right)$ is shown below:

$$\phi_s = \phi_{s_{max}} - \Delta\phi_{s_{supercritical}} * (1 - \Delta x)$$

$$where:$$

$$\Delta\phi_{s_{supercritical}} = \phi_{s_{max}} - \phi_{s_{supercritical}}$$

$$\Delta x = (Re_{crit} + \Delta Re_{supercritical}) - Re$$

This method produces the results in the curves shown in Figure 16 and matches the Achenbach wind tunnel data quite well over his tested range of Reynolds numbers and surface roughnesses.

References

Achebach, E. (1974) *The effects of surface roughness and tunnel blockage on the flow past spheres.* Journal of Fluid Mechanics, vol. 65, part 1. p. 113-125.

Brown, Frank N.M. (1971) *See The Wind Blow*. N.p.: (self Published), n.d. Print. F. N.M. Brown, Professor Emeritus, University of Notre Dame

Kensrud, Jeffrey Ryan. (2010*) Determining Aerodynamic Properties of Sports Balls In Situ.* Thesis. Washington State University.

Magnus, G. (1852) *On the Deviation of Projectiles; and on the Remarkable Phenomenon of Rotating Bodies*. Memoirs of the Royal Academy, p. 210-231

Mehta, Rabindra D. (2000) – *Cricket Ball Aerodynamics: Myth Versus Science*. NASA Techbooks.

Mehta, Rabindra D. and Pallis, Jani Marcari (2001) *Sports Ball Aerodynamics: Effects of Velocity, Spin, and Surface Roughness*. Materials and Science in Sports: p. 185-197

Mehta, Rabindra D. (2014) *Fluid Mechanics of Cricket Ball Swing*. Proc. of 19th Australasian Fluid Mechanics Conference, Australia, Melbourne.

Newton, Isaac. (1671-1672) *A letter of Mr. Isaac Newton, of the University of Cambridge, containing his new theory about light and color.* Philosophical Transactions of the Royal Society, vol. 7, p. 3075-3087.

Panton, Ronald L. (2005) *Incompressible Flow*. 3rd ed. Hoboken : John Wiley

Scobie, James A, Sangan, Carl M., and Lock, Gary D. (2014) *Flow visualization experiments on sports balls*. Procedia Engineering 72. p. 738-743.

Watts, Robert G., and Eric Sawyer. (1975) *Aerodynamics of a Kunckleball*. American Journal of Physics 43.11 p. 960-963.